





SERS Detection via Individual Bowtie Nanoantennas Integrated in Si_3N_4 Waveguides

Javier Losada, Ali Raza , Stéphane Clemmen, *Member, IEEE*, Aina Serrano, Amadeu Griol ,
Roel Baets , *Fellow, IEEE*, and Alejandro Martínez , *Senior Member, IEEE*

Abstract—Plasmonic resonances in metallic nanostructures provide a way for broadband enhanced light–matter interaction in subwavelength regions, which can be used to boost a variety of physical phenomena, notably including Raman scattering. Such nanostructures can be integrated on silicon chips and driven via dielectric waveguides, which may improve the performance of photonic integrated circuits in terms of foot-print, efficiency, sensitivity or power consumption, amongst other figures of merit. Here, we show that an isolated plasmonic nanoantenna can be efficiently integrated into a silicon nitride waveguide to detect surface-enhanced Raman scattering (SERS) spectra from molecular monolayers. We study numerically and experimentally two different configurations, both enabling the recording of Raman spectra at the output: nanoantenna on top of the waveguide and nanoantenna inserted in a subwavelength gap built in the waveguide. We also compare both configurations, which may pave the way toward massive integration of SERS devices for lab-on-a-chip applications.

Index Terms—Nanophotonics, plasmons, Raman scattering, silicon photonics.

I. INTRODUCTION

INTEGRATION of subwavelength-sized plasmonic nanostructures in silicon waveguides has received a considerable interest in the past few years. The main reason is that this hybrid plasmonic-photonic approach [1] reunites the best of

two worlds: on one side, the extreme optical properties of plasmonic nanostructures enabling a variety optical functionalities (sensing, modulation, non-linear processing) at low power and in sub-micron foot-prints; on the other side, the possibility of massive fabrication of photonic integrated circuits (PICs) using silicon-compatible technologies. A paradigmatic example of such a hybrid approach is the recent demonstration of a plasmonic electro-optic modulator integrated on a silicon waveguide which beats its dielectric counterparts in terms of speed, power consumption and foot-print [2].

One of the possible plasmonic structures to be integrated in silicon-based PICs is a metallic nanoantenna [3] supporting a localized surface plasmon resonance (LSPR) either in the near-infrared [4] or in the visible regime [5]. Either silicon or silicon nitride (Si_3N_4) waveguides are respectively chosen for each wavelength regime to ensure strong confinement in the waveguide core together with low propagation losses. In the simplest approach, plasmonic nanoantennas can be placed on top of the dielectric waveguides so that their excitation stems from the coupling between the evanescent part of the waveguide mode (usually, the fundamental TE-like mode) and the nanoantenna LSPR. This approach, which allows for both exciting the nanoantenna via the guided field and collecting the radiation that it scatters back to the coupled waveguide, has led to different interesting experimental results [4]–[11]. However, the weak coupling ($\sim 10\%$ at most) between the waveguide mode and the LSPR makes typically necessary to include a set of nanoantennas in order to observe a large contrast ratio at the waveguide output [5], [7]. The requirement for several antennas is a limiting factor obviously when probing single particles but also because it increases the propagation length into the Si_3N_4 core resulting in a much higher photon background radiation [10].

Plasmonic nanostructures play a key role in surface-enhanced Raman scattering (SERS), since the strong field localization in subwavelength volumes boost the efficiency of the Raman process by orders of magnitude [12]–[14]. Recently, the collection of SERS spectra from nanoantennas integrated on top of Si_3N_4 waveguides has been demonstrated, first by means of an array of nanoantennas to increase the amount of Raman scattering collected by the waveguides [15] and afterwards by means of a single nanoantenna by reducing the background noise in a backscattering detection scheme with short waveguide lengths [16].

Still, there is room for improvement, mainly in terms of excitation and collection efficiency, in the way towards single-molecule on-chip SERS spectrometry. A possible way

Manuscript received July 26, 2018; revised January 21, 2019; accepted January 22, 2019. Date of publication January 31, 2019; date of current version March 14, 2019. The work of A. Raza, S. Clemmen, and R. Baets was supported by the ERC Grant InSpectra and the FWO Belgium. The work of S. Clemmen was also supported by the F.R.S-FNRS. The work of A. Martínez was supported in part by the Spanish Ministry of Science, Innovation, and Universities (MICINN) under Grants TEC2014-51902-C2-1-R and TEC2014-61906-EXP and in part by the European Commission Project THOR H2020-EU-829067. (*J. Losada and A. Raza contributed equally to this paper.*) (*Corresponding author: Alejandro Martínez.*)

J. Losada, A. Serrano, A. Griol, and A. Martínez are with the Nanophotonics Technology Center, Universitat Politècnica de València, Valencia 46022, Spain (e-mail: jalofer@ntc.upv.es; aiserrad@ntc.upv.es; agriol@ntc.upv.es; amartinez@ntc.upv.es).

A. Raza and R. Baets are with the Photonics Research Group, INTEC Department, Ghent University, Ghent 9052, Belgium, and the Center for Nano- and Biophotonics, Ghent University, Ghent 9000, Belgium (e-mail: Ali.Raza@UGent.be; roel.baets@ugent.be).

S. Clemmen is with the Photonics Research Group, INTEC Department, Ghent University, Ghent 9052, Belgium, and also with the Laboratoire d'Information Quantique, Université Libre de Bruxelles, Bruxelles 1050, Belgium (e-mail: stephane.clemmen@ugent.be).

This paper has supplementary downloadable material available at <http://ieeexplore.ieee.org>, provided by the authors. This includes a PDF containing information relevant to the paper. This material is 559 KB in size.

Color versions of one or more of the figures in this paper are available online at <http://ieeexplore.ieee.org>.

Digital Object Identifier 10.1109/JSTQE.2019.2896200

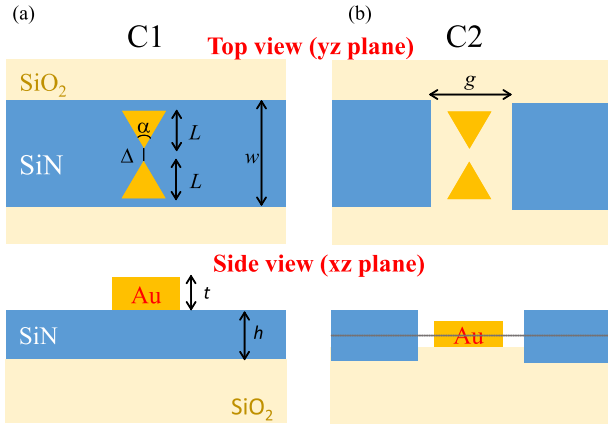


Fig. 1. Sketch of the two configurations under study. (a) The nanoantenna is placed on top of the waveguide so that its excitation is mediated by evanescent field coupling (C1). (b) The nanoantenna is placed in a gap created in the waveguide and aligned with the optical axis (C2).

to increase the coupling efficiency between the nanoantenna and the guided mode results from placing the nanoantenna in a subwavelength gap created in the waveguide, so that the nanoantenna is perfectly aligned with the waveguide optical axis [17]. In this approach, it can be considered that the nanoantenna is illuminated by a near-field probe (the waveguide facet) so the optical power delivered to the nanoantenna should be higher than in the on-top nanoantenna approach, thus enhancing the efficiency of the Raman process. However, this waveguide-gap approach has not been employed so far in SERS.

In this work, we demonstrate SERS via isolated bowtie Au nanoantennas integrated in Si_3N_4 waveguides using the two previous approaches: antenna on top and antenna in the gap. We show that both approaches enable to record SERS spectra from single nanoantennas but the gap approach performs better, which is supported by numerical results.

II. NUMERICAL STUDY

Figure 1 shows a sketch of the two configurations under study: nanoantenna on top of the waveguide (Fig. 1(a)) and nanoantenna inserted in a subwavelength gap in the waveguide (Fig. 1(b)). For simplicity, we term these configurations C1 and C2, respectively. In both cases, we consider Si_3N_4 waveguides with a rectangular cross-section ($w = 700$ nm and $t = 220$ nm) on a silica substrate and bowtie nanoantennas made of gold (Au).

There are two key parameters to model the performance of the structures in SERS [15]: the Raman enhancement factor and the β -factor. The Raman enhancement factor EF_R characterizes the excitation efficiency of the Raman centers. At a certain position, it can be obtained as $EF_R = I(\lambda_P)I(\lambda_S)$, where I stands for the optical intensity (or square of the electric field modulus $|E|^2$ in that position) and λ_P and λ_S are respectively the pump and Stokes wavelengths. Since plasmonic resonances are generally broad (optical Q factor ≈ 10 or bandwidths ≈ 100 nm at near infrared wavelengths), the intensity enhancement I at the pump and Stokes wavelengths are quite similar so EF_R is typically considered to be proportional to $|E|^4$ (the so-called ‘ E^4 law’ [13], [14]). In Ref. [15] the field normalization was carried out by comparing the field at the nanoantenna position (evanescent

field region over the top waveguide boundary) with and without nanoantenna. Since the nanoantennas are placed in different positions for each configuration, we will use the electric field at the center of the waveguide for normalization to ensure a fair comparison between both approaches. On the other hand, the β -factor models the amount of the Raman radiation that is coupled to the guided mode, and can be obtained as $\beta = P_{TE}/P_{rad}$, where P_{rad} is the total power radiated by a Raman center and P_{TE} is the power of the output guided mode. Noticeably, the analytical model developed in Ref. [15] for both parameters cannot be applied to C2, so here we use numerical simulations to compare the performance of both approaches.

We performed full-vectorial electromagnetic simulations using the software *CST Microwave Studio*. For both configurations we followed the same procedure: We used a non-dispersive refractive index of $n_{\text{SiN}} = 1.99$ for the waveguide core, $n_{\text{SiO}_2} = 1.45$ for the silica (SiO_2) undercladding and $n_{\text{air}} = 1$ for the air top cladding. We considered a thin layer of titanium as an adhesion layer between SiO_2 and Au. The metal stack thicknesses were fixed to $t_{\text{Ti}} = 2$ nm and $t_{\text{Au}} = 30$ nm, so $t = 32$ nm. An additional surface layer with thickness $t_{\text{MM}} = 1$ nm and index $n_{\text{MM}} = 3$ was used to model the molecular monolayer placed on top of the sample, as in Ref. [15]. The nanoantenna region (including the titanium adhesion layer and the monolayer) was meshed with a uniform mesh of 0.5 nm in the plane of the nanoantenna (yz -plane) and 1 nm in the x -direction. A mesh refinement to 0.5 nm was applied in regions where the thickness in the x -direction was ≤ 1 nm.

To calculate the intensity enhancement I at the nanoantenna surroundings, we placed an electric field monitor in the middle of the gap formed by the two bowtie arms at a height of 15 nm. For the β -factor calculations, we considered a fixed dipole emitter source positioned near the antenna surface, centered in the bowtie gap and at a height of 15 nm over the surface (this means, 45 nm over the substrate layer). P_{rad} can then be calculated using a 3D power monitor whose boundaries are in the far field of the dipole source. P_{TE} can be simultaneously determined using a monitor that extracts the power carried by the TE mode. Notice that even though the Raman centers will be placed at the metal surface, this calculations will give a qualitative view of the response of the whole system.

The nominal parameters of the C1 design were directly extracted from Ref. [15] and, therefore, not optimized: $\alpha = 60.51^\circ$, $\Delta = 20$ nm, $t = 30$ nm and $L = 120$ nm. C2 was designed to get the highest value of $EF(\lambda_P)^2$ in the wavelength region used in the experiments (around 780 nm). After the optimization step, the dimensions of the C2 nanoantenna were $\alpha = 64^\circ$, $\Delta = 35$ nm, $t = 30$ nm and $L = 120$ nm, for a waveguide gap of $g = 200$ nm.

Figure 2 depicts a comparison between both nominal designs, in terms of both $I(\lambda_P)$ (a) and the β -factor (b). It can be clearly seen that C2 performs better than C1 since both the Raman centers are excited more efficiently and the Raman excitation is more efficiently captured by the output waveguide. Especially, C2 provides a much higher field enhancement at the bowtie gap, as also shown in the electric field snapshots shown in Fig. 3. This can be attributed to two main reasons: first, because the plasmonic resonance seems to be red-shifted in C1; and second

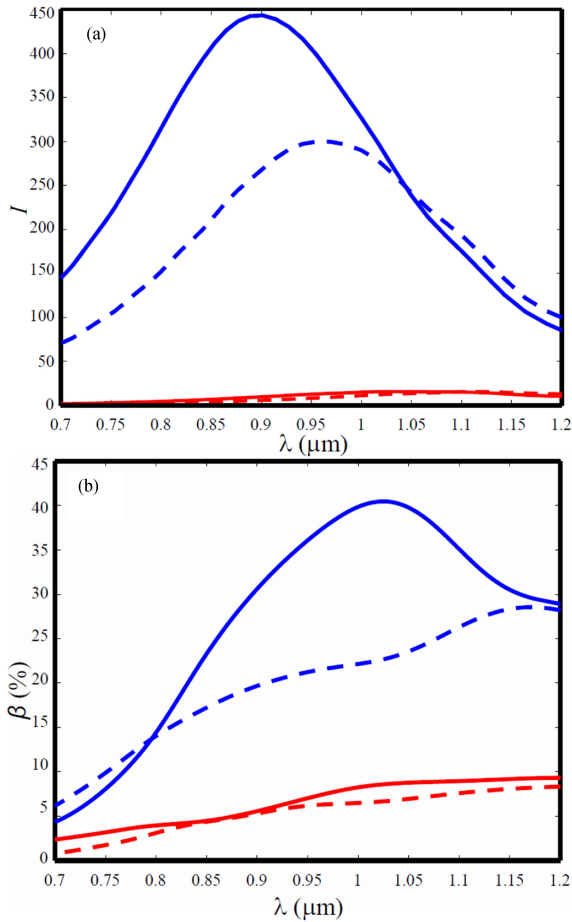


Fig. 2. Intensity enhancement factor $I(\lambda)$ (a) and β -factor (b) for both designs, C1 (red) and C2 (blue). Solid lines describe the response for ideally designed systems, whilst dashed lines show the response for the final fabricated systems (taking into account fabrication deviations).

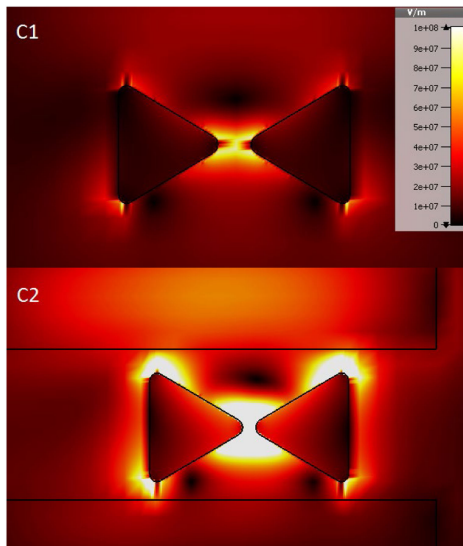


Fig. 3. Snapshots of the electric field at $\lambda = 876$ nm (roughly corresponding to the main Raman peak of the substance used in the experiments) around the nanoantenna region for both the C1 (top) and C2 (bottom) configurations. In both cases, the guided power is the same. The colorbar applies to both parts of the figure. See also Suppl. Movies S1 (for C1) and S2 (for C2).

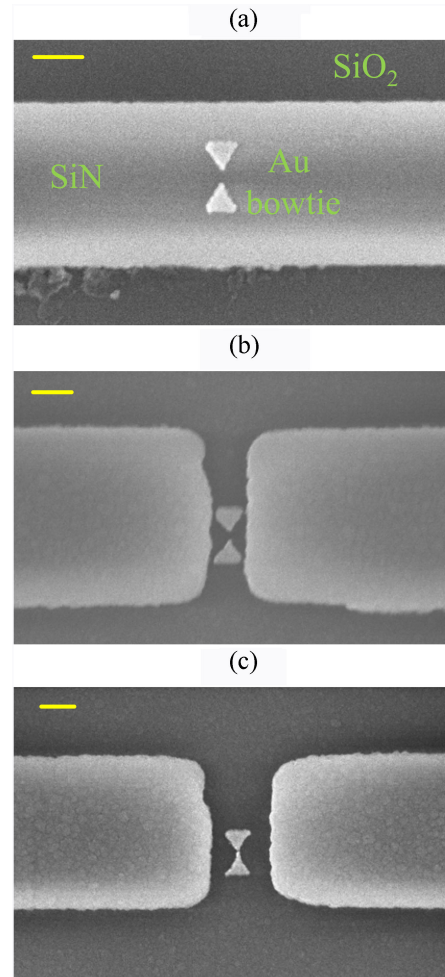


Fig. 4. SEM images of some of the fabricated samples: (a) C1, with $\Delta = 44$ nm; (b) C2 with $\Delta = 35$ nm and (c) with $\Delta = 0$ nm (the bowtie gap was not opened). The yellow line stands for 200 nm.

because the interaction between the guided fields is higher in C2 than in C1. As a result of the inaccuracies in the fabrication process, the dimensions of the real samples were different from the nominal designs (see Section III and, particularly, Fig. 4). Still, C2 is expected to be more efficient than C1, even though the performance of C1 could be certainly improved by designing the antenna to resonate closer to the pump wavelength.

III. FABRICATION

The samples for both C1 and C2 configurations were fabricated using standard silicon technology. As a starting material, a 200 mm Si wafer containing a stack of 2.3 ± 0.1 μm thick high-density plasma chemical vapor deposition SiO_2 and 220 nm thick plasma enhanced chemical vapor deposition (PECVD) Si_3N_4 is used [18]. First, the Si_3N_4 waveguides (with the gap for C2 samples) were fabricated. The fabrication process was based on an electron-beam direct-writing process performed on a 100-nm-thick poly(meth)acrylates (PMMA 905 K) resist film. The mentioned electron-beam exposure, performed with a Raith150 tool, was optimized in order to reach the required dimensions employing an acceleration voltage of 10 KeV and an

aperture size of 30 μm . After developing the PMMA resist using a mixture of IPA+MIBK, and in order to have an etching metal mask, a 20 nm chromium layer was evaporated prior to a lift-off process. Then, the waveguide patterns were transferred into the Si_3N_4 samples employing an optimized Inductively Coupled Plasma-Reactive Ion Etching process with fluoride gases. Finally, the remaining chromium layer was removed by using chromium etchant dissolution. For the C2 samples, an extra PECVD step for silica deposition (around 100 nm) on the whole sample was required in order to ensure the right height alignment between the antenna and the waveguide axis (see Fig. 1(b)).

Once the waveguides were fabricated, the Au bowtie structures were placed either on the waveguides (C1) or in the middle of the waveguide gaps (C2) by means of a second e-beam lithography process performed with the Raith150 tool prior to a new metal evaporation (30 nm of gold plus 2 nm of titanium for adhesion enhancement) and lift-off process. The PMMA thickness for the second exposure was ~ 100 nm, which is thick enough to ensure a right lift-off process of the metallic layer. The lift-off process was carried out in an Optiwet equipment using N-Methyl-2-pyrrolidone at 90 $^\circ\text{C}$ and a pressure of 60 bars. To ensure the right placement of the bowties, alignment marks, created in the previous Si_3N_4 etching level, and an iterative exposure process were used. Four samples were fabricated (one for C1 and three for C2) all of them containing a waveguide without nanoantenna for calibration purposes and seven waveguides with nanoantenna. Figure 4 shows scanning electron microscope (SEM) images of some of the fabricated samples. As mentioned in section II, the shape of the fabricated bowties was a little bit different from the nominal bowtie geometry because of fabrication inaccuracies. Indeed many of the bowties were not well formed (so they were not useful for characterization) and their bowtie aperture was different from the nominal one as shown in Fig. 3(a) and (b). Moreover, in some of the samples the bowtie gap was completely closed (Fig. 3(c)). The dimensions for fabricated antennas used in measurements were: $\alpha = 56.15^\circ$, $\Delta = 44$ nm, $t = 30$ nm and $L = 131.5$ nm (C1, Fig. 4(a)), and $\alpha = 59.71^\circ$, $\Delta = 35$ nm, $t = 30$ nm and $L = 135$ nm (C2, Fig. 4(b)). In addition, there is a certain misalignment with respect to the optical axis, which also was accounted for in the simulations. Still, we were able to excite the plasmonic resonances as shown in Section IV.

For SERS measurements, the fabricated chips were first cleaned using acetone + IPA + DI-water followed by O_2 plasma. Then 4-nitrophenol (pNTP) molecules in the form of a monolayer were bound to the metal surface of the nanoantenna by immersing the chip in a 1mM solution of pNTP in ethanol. After an overnight immersion, chips were thoroughly washed with ethanol and DI-water to remove the unbind pNTP molecules.

IV. EXPERIMENTAL RESULTS

We performed the SERS measurements using a commercial confocal Raman microscope (WITEC Alpha300R+). The schematic of the experimental setup is presented in Fig. 5(a). Figure 5(b) shows the input laser spot and the scattering from the single antenna. A $\lambda_P = 785$ nm excitation diode laser

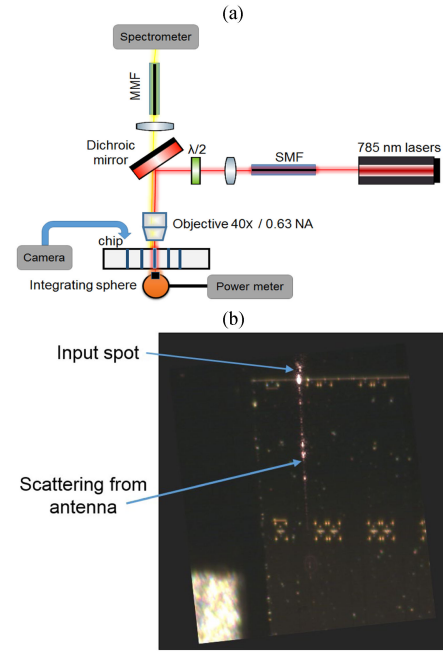


Fig. 5. (a) Schematic of the setup used for SERS measurements from nanoantennas integrated Si_3N_4 waveguides. (b) Input spot and the scattering from the single nanoantenna in experiments.

(Toptica XTRA II) is used as a pump source. The chip was placed underneath the objective (40 \times , 0.63 NA) so that TE mode of Si_3N_4 waveguide is excited via end-fire coupling. A low pump power of 1 mW (before objective) is used to avoid any material damage and subsequent photoreduction of pNTP. The coupling into the waveguide was optimized by looking simultaneously at the waveguide scattering using the top camera as well as at the expected 1339 cm^{-1} pNTP peak. All the Raman spectra were recorded with 1 sec integration time. The loss of the Si_3N_4 waveguide measured using cut back method is 3.2 ± 0.9 dB/cm. The coupling loss measured from the chip containing C1 and C2 configuration is 3.2 ± 0.5 and 3.0 ± 0.4 dB/facet, respectively. In this last case, we have assumed that the losses in the gap are ~ 2 dB, a value that has been obtained from numerical simulations. Further details about the experimental setup can be read from [16].

The measurement results are presented in Fig 6. Each spectrum is normalized by the coupling efficiencies to assure same pump power for both configurations. No NTP peak can be seen in the Raman spectrum measured from a reference waveguide (black). However, a strong NTP spectrum is present in the signal recorded from the waveguide functionalized with a single antenna (red). Apart from the expected pNTP Raman modes, a spurious Raman like background generated from the Si_3N_4 waveguide [10] is observed in all spectra. In the first set of measurements, the chip containing a set of waveguides with the bowtie on top (C1) is measured. For the best waveguide-antenna system (Fig. 4(a)) the Raman peak of the 1339 cm^{-1} mode ($\nu_s(\text{NO}_2)$) is visible in Fig 6(a). However, due to the low excitation and collection efficiency (β -factor), no other Raman modes are present. In the second set of the measurements, the set of samples with antennas in the gap (C2) was explored. The same pump power, integration time and CCD setting were used.

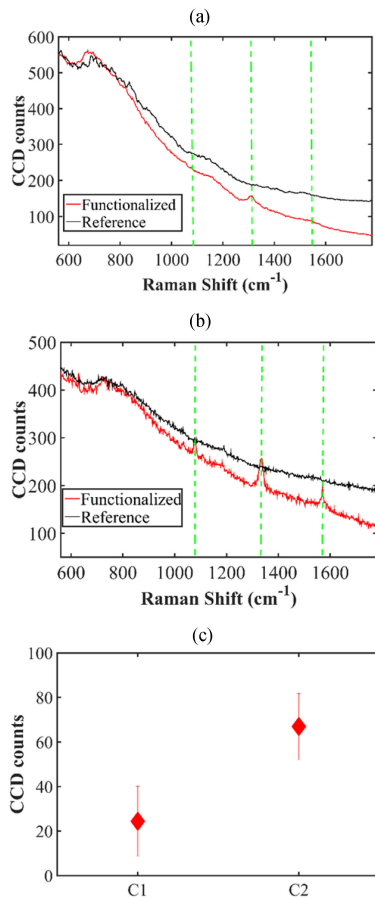


Fig. 6. The Raman spectrum measured from the waveguides functionalized with single antenna for (a) C1 and (b) C2. The green dotted line represents the NTP Raman modes, i.e., 1080, 1339, and 1575 cm^{-1} . (c) The CCD counts corresponding to 1339 cm^{-1} Raman mode of NTP.

As shown in Fig 6(b), aside from 1339 cm^{-1} Raman modes, two more peaks at 1076 cm^{-1} and 1580 cm^{-1} (benzene ring vibrations) also appear in the Raman spectra. The higher noise in Fig 6(b) is attributed to higher coupling loss. In Fig 6(c), we compare the Raman signal strength measured from both antenna configurations. For the same pump power and integration time, the Raman signal recorded for C2 is at least three times stronger than in C1, where both antennas geometries were optimized for highest signal strength. It is worth mentioning that no Raman peaks appeared in the recorded spectra of the samples before the pNTP functionalization was performed.

These experimental results are supported by the numerical predictions: being the intensity enhancement and the β -factor about two and one orders of magnitude higher in C2 than in C1, we could expect a much better resolved Raman spectrum in C2. In this sense, it is worth mentioning that C1 is far from being optimized and the bowtie plasmonic resonance is redshifted beyond 1 μm , so in an optimum configuration with the resonance close to the pump laser the C1 structure would potentially enable to record also all the Raman peaks, as shown in [16].

V. CONCLUSION

In this work, we have demonstrated that the marriage between silicon photonics and plasmonics may give rise to new

devices for advanced on-chip chemical spectroscopy. In particular, single plasmonic nanoantennas with a sub-micron square foot-print, well below what can be achieved using dielectric structures, can enormously concentrate incoming guided fields to excite Raman centers whose emitted radiation is also efficiently collected by output waveguides.

Next steps should include the increase of the field localization (higher values of I) via narrower gaps (<10 nm) in the nanoantenna, which should eventually lead to single-molecule spectroscopy [19] on silicon chips. Such narrowing could be performed by alternative methods in which the gap is not defined lithographically but by self-assembly, as recently demonstrated in plasmonics picocavities following a nanoparticle-on-mirror structure [20]. Ways for enhancing the collection of the Raman radiation by the output waveguide have to be addressed, especially for the C2 configuration where the distance from the nanoantenna to the output waveguide facet should be as small as possible in order to capture the maximum amount of emitted radiation.

In the way towards commercialization, CMOS compatibility should also be considered. In this case, the replacement of Au (not CMOS compatible) by CMOS-compatible plasmonic materials [21] such as titanium nitride [22] or copper [23] would be mandatory. By additionally using multiple waveguides with integrated antennas, which could be simultaneously excited by a single laser, it would be feasible to perform Raman spectroscopy of multiple substances in ultra-compact and low-cost SERS chips.

ACKNOWLEDGMENT

The authors would like to thank Prof. A. Skirtach (UGent, Belgium) for his support in experiments. The authors would also like to thank Dr. F. Peyskens (UGent, Belgium/Quantum Photonics Laboratory, RLE, MIT, USA) for useful discussion.

REFERENCES

- [1] F. J. Rodríguez-Fortuño, A. Espinosa-Soria, and A. Martínez, "Exploiting metamaterials, plasmonics and nanoantennas concepts in silicon Photonics," *J. Opt.*, vol. 18, pp. 123001–123014, 2016.
- [2] C. Haffner *et al.*, "Low-loss plasmon-assisted electro-optic modulator," *Nature*, vol. 556, pp. 483–486, 2018.
- [3] L. Novotny and N. F. van Hulst, "Antennas for light," *Nature Photon.*, vol. 5, pp. 83–90, 2011.
- [4] I. Alepuz-Benache *et al.*, "Strong magnetic resonance of coupled aluminum nanodisks on top of a silicon waveguide," *Proc. SPIE*, vol. 8424, 2012, Art. no. 84242J.
- [5] F. Peyskens *et al.*, "Bright and dark plasmon resonances of nanoplasmonic antennas evanescently coupled with a silicon nitride waveguide," *Opt. Express*, vol. 23, no. 3, pp. 3088–3101, 2015.
- [6] F. Bernal Arango, A. Kwadrin, and A. F. Koenderink, "Plasmonic antennas hybridized with dielectric waveguides," *ACS Nano*, vol. 6, no. 11, pp. 10156–10167, 2012.
- [7] M. Février *et al.*, "Giant coupling effect between metal nanoparticle chain and optical waveguide," *Nano Lett.*, vol. 12, no. 2, pp. 1032–1037, 2012.
- [8] M. Chamanzar, Z. Xia, S. Yegnanarayanan, and A. Adibi, "Hybrid integrated plasmonic-photonics waveguides for on-chip localized surface plasmon resonance (LSPR) sensing and spectroscopy," *Opt. Express*, vol. 21, no. 26, pp. 32086–32098, 2013.
- [9] J. Cuadra *et al.*, "Hybrid dielectric waveguide spectroscopy of individual plasmonic nanoparticles," *AIP Adv.*, vol. 7, 2017, Art. no. 075207.
- [10] N. Le Thomas, A. Dhakal, A. Raza, F. Peyskens, and R. Baets, "Impact of fundamental thermodynamic fluctuations on light propagating in photonic waveguides made of amorphous materials," *Optica*, vol. 5, no. 4, pp. 328–336, 2018.

- [11] B. Chen *et al.*, "Hybrid photon–plasmon coupling and ultrafast control of nanoantennas on a silicon photonic chip," *Nano Lett.*, vol. 18, pp. 610–617, 2018.
- [12] S. M. Nie and S. R. Emery, "Probing single molecules and single nanoparticles by surface-enhanced Raman scattering," *Science*, vol. 275, pp. 1102–1106, 1997.
- [13] K. Kneipp *et al.*, "Single molecule detection using surface-enhanced Raman scattering (SERS)," *Phys. Rev. Lett.*, vol. 78, pp. 1667–1670, 1997.
- [14] P. Roelli, C. Galland, N. Piro, and T. J. Kippenberg, "Molecular cavity optomechanics as a theory of plasmon-enhanced Raman scattering," *Nature Nanotechnol.*, vol. 11, pp. 164–169, 2016.
- [15] F. Peyskens, A. Dhakal, P. Van Dorpe, N. Le Thomas, and R. Baets, "Surface enhanced Raman spectroscopy using a single mode nanophotonic-plasmonic platform," *ACS Photon.*, vol. 3, no. 1, pp. 102–108, 2016.
- [16] F. Peyskens, P. Wuytens, A. Raza, P. Van Dorpe, and R. Baets, "Waveguide excitation and collection of surface-enhanced Raman scattering from a single plasmonic antenna," *Nanophotonics*, vol. 7, no. 7, pp. 1299–1306, 2018.
- [17] A. Espinosa-Soria, A. Griol, and A. Martínez, "Experimental measurement of plasmonic nanostructures embedded in silicon waveguide gaps," *Opt. Express*, vol. 24, pp. 9592–9601, 2016.
- [18] A. Z. Subramanian *et al.*, "Low-loss singlemode PECVD silicon nitride photonic wire waveguides for 532–900 nm wavelength window fabricated within a CMOS pilot line," *IEEE Photon. J.*, vol. 5, no. 6, Dec. 2013, Art. no. 2202809.
- [19] R. Zhang *et al.*, "Chemical mapping of a single molecule by plasmon-enhanced Raman scattering," *Nature*, vol. 498, pp. 82–86, 2013.
- [20] F. Benz *et al.*, "Single-molecule optomechanics in picocavities," *Science*, vol. 354, pp. 726–729, 2016.
- [21] G. V. Naik, V. M. Shalaev, and A. Boltasseva, "Alternative plasmonic materials: Beyond gold and silver," *Adv. Mater.*, vol. 25, no. 24, pp. 3264–3294, 2013.
- [22] G. V. Naik, J. L. Schroeder, X. Ni, A. V. Kildishev, T. D. Sands, and A. Boltasseva, "Titanium nitride as a plasmonic material for visible and near-infrared wavelengths," *Opt. Mater. Express*, vol. 2, pp. 478–489, 2012.
- [23] D. Y. Fedyanin, D. I. Yakubovsky, R. V. Kirtaev, and V. S. Volkov, "Ultralow-loss CMOS copper plasmonic waveguides," *Nano Lett.*, vol. 16, pp. 362–366, 2016.

Javier Losada received the B.S. degree in electrical engineering and the M.S. degree in advanced electrical engineering in 2014 and 2016, respectively, both from Universidad de Extremadura (UEX), Badajoz, Spain. He is currently working toward the Ph.D. degree in telecommunications with the Polytechnic University of Valencia, Valencia, Spain. He developed his Master thesis at SPEAG Company, Zurich, Switzerland, on the topic of Computational optics, specifically focused on the design of advanced boundary condition for optical simulations. His current research interests include plasmonics, metamaterials, nonlinear phenomena, and quantum physics.

Ali Raza received the B.Sc. degree in engineering sciences (photonics engineering) from the Ghulam Ishaq Khan Institute of Engineering Sciences and Technology, Topi, Pakistan, and the M.Sc. degree in photonics sciences from the University of Eastern Finland, Kuopio, Finland, in 2015. He is currently working toward the Doctoral degree with Photonics Research Group, Ghent University, Ghent, Belgium. He is working on waveguide-enhanced and surface-enhanced Raman spectroscopy on SiN platform. During bachelors, he did research internships at British American Tobacco and Attock Oil Refinery. During his masters, he also did a research internship at DESY, Hamburg, Germany.

Stéphane Clemmen (M'15) was born in Charleroi, Belgium, in 1983. He received the B.S. and M.S. degrees in physics from the University of Brussels, Brussels, Belgium, from where he received the Ph.D. degree in physics in 2010. After graduation in 2010, he joined Cornell University (NY) for four years as a Postdoctoral Researcher in the Quantum and Nonlinear Photonics Group. From 2014 to 2017, he was with the Photonics Research Group, University of Ghent (Belgium), as a Postdoctoral Researcher. In 2017, he has been granted a research mandate from the FNRS (Belgium) and is back to his alma mater in Brussels. He is also currently a Professor specialized in quantum photonics at Ghent University (Belgium). He has more than 20 publications in peer-reviewed journals and more than 35 contributions to conferences. His research interests include quantum photonics, nonlinear optics, on-chip spectroscopy, and integrated optics.

Aina Serrano received the Engineer degree in material science in 2014 and the Master's degree in mechanical engineering in 2017, both from Universitat Politècnica de València (UPV), Valencia, Spain. Since 2015, she has been working with Valencia Nanophotonics Technology Center (NTC), Spain. After her experience in microfabrication area working on silicon integrated photonics and plasmonic-based sensors, she joined the Assembly and Packaging Laboratory. She is currently involved in R&D European projects and collaborates with different microelectronic companies, developing packaging processes for the integration of photonic devices, such as die and flip-chip bonding, pigtail, and wire bonding.

Amadeu Griol was born in València, Spain, in 1973. He received the Telecommunication Engineer and Ph.D. degrees from the Universitat Politècnica de València in 1998 and 2003, respectively. His research interests include fabrication, modeling, and characterization of electrical and optical devices, especially microwave microstrip filters with harmonic suppression techniques and also photonic integrated circuits and nanophotonic devices for communication as well as biosensing applications. He has been working for more than ten years in the fabrication of optical micro- and nanodevices by using electron beam lithography techniques. He has been involved in several FP6, FP7, and H2020 European projects in charge of optical devices micro- and nanofabrication tasks. He authored and coauthored more than 50 papers in international journals, more than 100 contributions to international conferences and 2 patents.

Roel Baets received the M.Sc. degree in electrical engineering from Ghent University (UGent), Ghent, Belgium, in 1980, a second M.Sc. degree from Stanford University, Stanford, CA, USA, in 1981, and the Ph.D. degree from UGent in 1984.

He is a Full Professor with (UGent) and is associated with IMEC. From 1984 till 1989, he held a postdoctoral position at IMEC. Since 1989, he has been a Professor in the Faculty of Engineering and Architecture, UGent, where he founded the Photonics Research Group. From 1990 till 1994, he has also been a part-time Professor with the Delft University of Technology and from 2004 to 2008 with the Eindhoven University of Technology. He has mainly worked in the field of integrated photonics. He has made contributions to research on photonic integrated circuits, both in III–V semiconductors and in silicon, as well as their applications in telecom, datacom, sensing, and medicine. Web of Science reports more than 600 publications with an h-index over 60.

As a part of a team of eight professors, he leads the Photonics Research Group. With about 90 researchers, this group is involved in numerous (international) research programs and has created four spin-off companies. The silicon photonics activities of the group are part of a joint research initiative with IMEC.

He has led major research projects in silicon photonics in Europe. In 2006, he founded ePIXfab, the globally first multi-project-wafer service for silicon photonics. Since then ePIXfab has evolved to become the European Silicon Photonics Alliance. He is also the Director of the Multidisciplinary Center for Nano- and Biophotonics, UGent, founded in 2010. He was a co-founder of the European M.Sc. programme in Photonics.

He is an ERC grantee of the European Research Council and a Methusalem grantee of the Flemish government. He is a Fellow of the European Optical Society and the Optical Society. He is also a member of the Royal Flemish Academy of Belgium for Sciences and the Arts.

Alejandro Martínez (M'01–SM'14) received the Telecom Engineer B.Sc. and Ph.D. degrees from the Universidad Politècnica de Valencia (UPV), Valencia, Spain, in 2000 and 2004, respectively. His Ph.D. thesis was focused on passive optical devices based on two-dimensional photonic crystals. Since 2017, he has been a Full Professor with the Universidad Politècnica de Valencia. He is leading the "Plasmonic Metamaterials" research line at the Nanophotonics Technology Center, Valencia, Spain. He has co-authored more than 100 papers in international peer-reviewed journals and holds 8 patents. He has been the PI of several projects and contracts funded by some of the most important European funding agencies: 2 FP7 projects, 2 contracts with ESA, and 2 contracts with EDA. Besides, he has also been the PI in seven Spanish projects of the most competitive calls. He is a Senior Member of the OSA. His research interests include cavity optomechanics, plasmonics, nanoantennas, and metamaterials and its integration into silicon photonics chips.